

Simultaneous Ocean Wave Measurements by the Jason and Topex  
Satellites, With Buoy and Model Comparisons

R. D. RAY

Space Geodesy Branch, NASA Goddard Space Flight Center  
Greenbelt MD 20771, USA

B. D. BECKLEY

Raytheon ITSS, NASA/GSFC, Code 971  
Greenbelt MD 20771, USA

Corresponding author:

Richard D. Ray  
NASA/GSFC, Code 926  
Greenbelt, MD 20771  
USA

tel: (301) 301-6102

fax: (301) 614-6099

email: [richard.ray@gsfc.nasa.gov](mailto:richard.ray@gsfc.nasa.gov)

June 11, 2003

*The verification phase of the Jason-1 satellite altimeter mission presents a unique opportunity for comparing near-simultaneous, independent satellite measurements. We here examine simultaneous significant wave height measurements by the Jason-1 and Topex/Poseidon altimeters. These data are also compared with in-situ measurements from deep-ocean buoys and with predicted wave heights from the WaveWatch III operational model. The rms difference between Jason and Topex wave heights is 21 cm, and this can be further lowered by application of median filters to reduce high-frequency noise. This noise is slightly larger in the Jason dataset, amounting to about 7 cm rms for frequencies above 0.05 Hz, which is the frequency at which the coherence between Topex and Jason measurements drops to zero. The probability density function for Jason shows a dearth of small waves relative to Topex. Buoy comparisons confirm that this problem lies with the Jason measurements. The buoy comparisons confirm previous reports that Topex wave heights are roughly 5% smaller than buoy measurements for waves between 2 and 5 m; Jason heights in general are 2.7% smaller than Topex. Spurious dips in the Topex density function for 3- and 6-meter waves, a problem that has existed since the beginning of the mission, can be solved by waveform retracking.*

---

**Keywords** ocean waves, satellite altimetry, significant wave height, Jason-1 validation.

## **Introduction**

Over the past decade satellite altimetry has become an indispensable tool for observing global ocean waves (Lefevre & Cotton, 2001). The data are routinely used in numerical wave prediction programs, either for model tuning and validation or for direct assimilation (e.g., Lionello & Janssen,

1992; Bauer et al., 1996; Bidlot et al., 2002). Moreover, the nature of the altimeter observing system provides the only mechanism for obtaining wave measurements of a global nature and over extended periods of time. This is essential for studies of climate variability (e.g., Bacon & Carter, 1991; Wang and Swail, 2001). Altimetric measurements of wave heights, of course, also provide an essential component to altimeter measurements of sea level through the electromagnetic or sea-state bias corrections.

For these applications, and especially for the subtle variations associated with climate variability, it is critical that careful calibration and validation studies be performed. The present paper is one contribution to the calibration and validation of the significant wave heights measured by the Jason-1 satellite, the successor mission to Topex/Poseidon (T/P), launched 7 December 2001.

The verification phase of the Jason-1 mission provides a unique opportunity for such a study. For a period of about six months, from late January through mid-August 2002, the Jason-1 and T/P satellites were flying in formation along the same ground-track, separated in time by only about 70 seconds. Such near-simultaneous measurements allow these two systems to be compared and calibrated against one another in an unprecedented manner.

This paper is concerned exclusively with the altimeter data collected during the Jason verification phase. In addition, we compare the altimeter measurements during that period with *in situ* wave measurements from a collection of deep-ocean buoys and with numerical predictions from an operational wave model. Earlier T/P altimeter data have been compared with various buoy data by Gower (1996) and by others. The wave model used here is the NOAA WaveWatch III operational model described by Tolman (1999) and Tolman et al. (2002).

The relevant parameter of interest here is the significant wave height, estimated from the slope of the leading edge of the altimeter's returned wave form (Fedor et al., 1979). Because significant

wave height is defined as the average of the largest one-third waves, it is sometimes descriptively denoted  $\overline{H_{1/3}}$ , but we here use the simpler  $H_s$ . Some details concerning Jason-1  $H_s$  data processing procedures may be found in the report by Dumont et al. (2001).

## Data

The Jason-1 altimeter data available for this study were obtained from so-called Interim Geophysical Data Records (IGDRs) created by Centre National d'Études Spatiales (CNES) and obtained from the Physical Oceanography data archiving center (PODAAC) at the Jet Propulsion Laboratory. The T/P data in GDR format were also obtained through PODAAC.

We use the first 18 full ten-day repeat cycles, which are labeled Jason cycles 3 through 20, beginning 4 February 2002 and ending 1 August 2002. The corresponding T/P cycles are 346 through 363. Throughout this period the Topex altimeter was functioning with its "Side B" electronics. During T/P cycle 361 the spacecraft was operating with the Poseidon rather than the Topex altimeter, and these data are not used. In addition, some highly anomalous  $H_s$  data were identified throughout Jason cycle 8 and the data from this cycle are also not used. In this paper we examine only the Ku-band wave data; wave data are also available from the C-band ranges, but the C-band data are significantly noisier and are therefore not used. Although Quartly (1997) shows how C-band data can be usefully employed to improve rain-contaminated  $H_s$  estimates, his approach requires retracking which we have not done.

We do have access, however, to one experimental retracking dataset for the Topex altimeter. The dataset was created as part of a Topex-Jason "compatibility" project by P. Callahan (personal communication, 2002) following methods described by Rodríguez and Martin (1994). At the time of this writing, these retracked Topex data are available only for the period of the Jason verification.

We include these data in many of our comparisons below, but, in general, when we refer to “Topex” we refer to the original data which are consistent with the  $H_s$  data generated throughout the mission (or, strictly, with the data obtained since the altimeter was switched to Side B).

Wave model data were obtained from NOAA’s WaveWatch III system, a third-generation operational wave forecasting program running at the National Center for Environmental Prediction (NCEP) and employing NCEP operational surface wind and air-sea temperature fields and polar ice concentrations as input. Like all third-generation systems it numerically integrates equations describing the wave energy spectrum in space and time. Significant wave height  $H_s$  is estimated from the integrated energy spectrum. The  $H_s$  fields are available on a near-global grid of resolution  $1.25^\circ$  (longitude)  $\times$   $1^\circ$  (latitude), every 3 hours. Further detailed information, including comparisons with other third-generation systems and with wave measurements, is given by Tolman et al. (2002) and references therein. The model does not assimilate wave data, so the model output is completely independent of the satellite altimeter data with which it is compared below.

### Comparisons Along a Single Track

The general character of the satellite  $H_s$  data can be seen in Figure 1, which shows a long, nearly continuous track crossing the Pacific Ocean and extending through the Drake Passage and into the South Atlantic. At the broadest scales one notices the very typical enhancement of wave energy throughout the Southern Ocean. At smaller scales there is considerable fine structure: features with wavelengths smaller than a few hundred km and amplitudes a fraction of a meter are distinctly recognizable. There are a few evident outliers and a general high-frequency noise envelope of roughly 10 cm, but the noise is sufficiently low to allow a rich signal to be observed. The character of the high-frequency noise is somewhat clearer in the zoom view of the lower panel.

Along this particular track the Topex and Jason data agree well, with rms difference of 17 cm and no obvious long-wavelength discrepancies. The coherence between the two measurements is shown in Figure 2. (For this calculation the outliers evident in Figure 1 have been manually removed and the few gaps filled by linear interpolation.) The high coherence begins to degrade sharply at frequencies above 0.025 HZ (i.e., distances shorter than approximately 200 km) and the coherence drops to insignificance above 0.05 HZ (about 100 km). At frequencies above 0.05 Hz the integrated spectral energy density is  $156 \text{ cm}^2$  for Jason and  $106 \text{ cm}^2$  for Topex. That is, the Jason data are noisier by roughly 7 cm. Both variances are higher than the 3 cm rms noise inferred by Monaldo (1988) from the white-noise floor of the  $H_s$  spectrum (measured, in that case, by Geosat), but determining at what frequency a noise floor is reached is not always obvious. In addition to this high-frequency noise, the Jason data, in this track as well as in general, have a somewhat greater number of outliers than Topex. We have found it beneficial to apply a median filter to the 1-Hz  $H_s$  data, of width about 11 samples. The filter acts to eliminate most outliers as well as to reduce the high-frequency noise.

The wave model data shown in Figure 1 have been interpolated bilinearly in space and linearly in time to the satellite space-time location. The interpolated result is seen to agree fairly well with the altimetry throughout most of this pass except for the largest waves around time 5500 s, which corresponds to passage through the Drake Passage. The wave model is known to be slightly less accurate at higher latitudes (Tolman et al., 2002), and the region surrounding the Drake Passage presents special challenges owing to its complex shape and nearby island chain, long fetch, and relatively less accurate operational wind fields. Over the entire track shown in Figure 1, the rms difference between the model and the Jason data is 47 cm. More general global statistics are given below.

## Global Comparisons

The figures and tables of this section derive from over 6 million 1-Hz  $H_s$  measurements made over the course of the Jason verification campaign. The data are global, but somewhat weighted toward higher latitudes owing to the pattern of the T/P and Jason ground-tracks (turning latitude at  $66^\circ$ ).

### *One-dimensional Density Functions*

Figure 3 shows the observed probability density functions over this time period, for both the original and retracked Topex data, for the Jason data, and for the numerical model. Corresponding statistical data are summarized in Table 1.

The mean Topex and Jason wave heights differ by about 9 cm, with the Topex mean the larger, but this discrepancy is halved for the retracked Topex data. The median heights are slightly more consistent among all three datasets, and the modes agree within  $\pm 2$  cm.

In Figure 3 the most noticeable difference between Topex and Jason is a dearth of small waves in the Jason dataset. In fact, rarely is a Jason  $H_s$  measurement less than 50 cm (discounting the anomalous data in cycle 8). Given that the real ocean not only has small waves, but that measurement error would also tend to widen the real distribution and augment the observed density of small waves, this lack of low- $H_s$  data must be the result of inadequacies in the model used for Jason waveform tracking. Further evidence for this statement is given below.

Figure 3 also shows that retracking of Topex data solves the spurious dips in the Topex density function that occurs near  $H_s = 3$  and 6 meters. These dips have been present since the beginning of the mission (see Figure 1 of Callahan et al., 1994). They are the result of slightly inadequate correction tables for pointing angle and sea-state effects in  $H_s$  estimates; each gate index has a

separate correction, and the dips are seen to occur at gate boundaries (which on Topex occurs at 0.9, 2.9, 6.2, and 13.0 m). The Topex retracking clearly solves this problem. Otherwise, the original and retracked Topex density functions are very similar.

The probability density of the model  $H_s$  predictions is impressively close to the altimeter results. The density is slightly shifted rightwards, with somewhat fewer 1-meter waves and somewhat more 3 and 4-meter waves. The mean is shifted higher accordingly (see Table 1). The standard deviation of the model heights is in very close agreement to the standard deviations of the altimeter heights (see Table 1). The distribution is slightly more normal-like, i.e., slightly lower skewness and kurtosis.

The smooth, dotted lines in Figure 3 are identical in all four panels, which is designed to facilitate comparisons among the four observed densities. These dotted lines are in fact the density function of a generalized extreme value distribution (Johnson et al., 1995), fit by the maximum likelihood method (Hosking, 1985) to the retracked Topex distribution. Various probability distributions have been proposed to model  $H_s$ , probably the most common being the lognormal (e.g., Bauer and Staabs, 1998). Ochi (1998) advocates a generalized gamma distribution, but he also points out that, because of the wide range of sea states and conditions around the globe, there is no scientific basis for selecting one particular distribution to describe  $H_s$  in general. Hence, our global probability distribution is necessarily a mixture of many distributions and, in addition, must be the result of convolution with some sort of error model that describes measurement error.

We find that the extreme value function gives a somewhat more satisfactory fit to the retracked Topex data of Figure 3 than do the generalized lognormal and generalized gamma distribution functions. The density function of an extreme-value distribution is given by (Johnson et al., 1995; Hosking and Wallis, 1997)

$$\text{pdf}(x) = \alpha^{-1} \exp(-(1-k)y - e^{-y}) \quad (1)$$

where

$$y = -k^{-1} \log\{1 - k(x - \xi)/\alpha\}$$

where  $\alpha$ ,  $k$ , and  $\xi$  are free parameters describing scale, shape, and location, respectively. (Taking  $k = 0$  gives a Gumbel distribution, used by Tournadre (1993).) The dotted lines in Figure 3 are given by  $\alpha = 100$ ,  $k = -0.05$ , and  $\xi = 204$  when  $x$  is in cm. While the agreement of this function with the data is not especially impressive, it is sufficient for present purposes, which are: (1) to facilitate comparisons among the panels of Figure 3 and (2) to facilitate some Monte Carlo simulations for which exact agreement with the observed density is not needed.

The cumulative distribution functions for Topex and Jason are shown in Figure 4. These functions are plotted on “lognormal paper” so that a real lognormal distribution would fall on a straight line. One sees that for the great majority of data the distributions are indeed lognormal, but not for small or large waves. As probability approaches 1, such curves are often used to predict the occurrence rate for extreme events, so the mismatch there is important. For the same reason, the agreement between Jason and Topex in this region of the diagram is reassuring. Using buoy measurements, Ochi (1998) finds that the lognormal typically underpredicts the occurrence of both very small and very large waves, a conclusion consistent with the Topex curve, although measurement error may cause the Topex curve to be biased high for small waves. Figure 4 again emphasizes the lack of small waves in the Jason dataset.

#### *Two-dimensional Density Functions*

The joint probability density observed by the two altimeter systems is shown in Figure 5. The rms difference between Topex and Jason measurements in this figure is 21 cm, of which a significant part is explained by the mean difference of about 9 cm. The distribution of data in Figure 5 is

already remarkably tight, given the near-logarithmic scale of the contouring, but there is a subtle bowing of contours away from the diagonal near 2 meters where some fraction of the Jason data are anomalously high. Presumably this further reflects occasional outliers in the Jason data. With median filtering applied, the rms drops to 14.5 cm.

In Figure 5 the contours at small wave height are distorted, as if compressed from the left, which again reflects the dearth of small waves in the Jason dataset. The abrupt compression is clearly unnatural and suggests, even without further evidence, that the fault lies with the Jason data.

Figure 5 also clearly shows most Topex wave heights slightly larger than Jason, with an additional suggestion of a linear trend. This is seen more strikingly in Figure 6 where the difference in wave heights is plotted in exaggerated manner on the vertical axis. The discrepancy, although approximately described by a straight line, is actually nonlinear, because the main axis of the contours levels off at high wave heights. The distortion at small wave heights is also nonlinear. Nonetheless, Figures 5 and 6 suggest that a linear approximation might be employed as a correction to yield a more consistent dataset for the two satellites. Based on buoy comparisons, Lefèvre and Cotton (2001) advocate a linear correction to Topex data which increases the observed data by roughly 5% of  $H_s$ ; Jason data would thus require a slightly larger adjustment.

A linear fit to the data of Figure 5 must account for the fact (which classical regression methods do not) that errors are present in both variables (e.g. Madansky, 1959). Because the independent variable (be it Jason or Topex heights) may be thought of as a random variable, the theory of linear structural relationships (Moran, 1971; Cheng and Van Ness, 1999) is applicable. (With some justification, Caires and Sterl (2003) consider the problem a functional, rather than structural, relationship, but the practical consequences of that are here irrelevant.) To make progress some

knowledge of the error variances (e.g., their ratio) is required. Although our spectral estimates suggest that Jason data may be slightly more noisy than Topex, we here for simplicity assume identical errors in both systems. Under an additional assumption that the distribution of the independent variable is normal, then maximum-likelihood errors-in-variables regression, orthogonal regression, and principal components regression (used by Bauer and Staabs, 1998) yield identical results. We here employ orthogonal regression. While the distribution of  $H_s$  is not normal, regression results are not unduly sensitive to this, and orthogonal regression yields correct estimates which we have checked by Monte Carlo simulations. Under these assumptions the straight line in Figure 6a, corresponding to a linear relationship of form

$$H_s^{\text{Topex}} = \beta_1 H_s^{\text{Jason}} + \beta_0 \quad (2)$$

is given by

$$\beta_1 = 1.027 \quad \beta_2 = 1.8 \text{ cm.}$$

(Here  $\beta_1$  is the reciprocal of that listed in Table 2.) The standard errors in both  $\beta_i$  estimates are smaller than the quoted precisions, even allowing for reasonably high serial correlation in the data. Moreover, cycle-by-cycle regressions show a standard deviation in the estimated slope of 0.0016, and, of course, the standard error in the mean is smaller yet. Note that an ordinary least squares fit that assumes no error in the independent variable gives a slope of either 1.016 or 1.037, depending on which satellite measurement is taken as the independent variable. Orthogonal regression estimates always fall between these two extremes.

A linear adjustment to the data according to Equation (2), combined with median filtering of the original  $H_s$  data, reduces the 21-cm rms difference between Topex and Jason to 10.7 cm. This

is very nearly the precision of the original Topex data.

For Figure 6b, which compares Jason with retracked Topex data, the linear relationship (2) is given by

$$\beta_1 = 1.037 \quad \beta_2 = -4.7 \text{ cm.}$$

The residual rms in this case is slightly lower, 10.3 cm, perhaps because the distortions near 3-m and 6-m waves, very evident in Figure 6a, are rectified in Figure 6b.

The corresponding joint density between Jason  $H_s$  measurements and the WaveWatch numerical model is shown in Figure 7. The data spread is considerably greater than that in Figure 5, reflecting an overall poorer level of agreement, yet several aspects of the two diagrams are similar: (1) the distortion at small wave heights caused by the lack of small Jason waves and (2) the locus of maximum density lying along an approximate straight line with slope greater than unity.

Several statistics summarizing the differences among Topex, Jason, and model heights are given in Table 2. They are consistent with the one-dimensional and two-dimensional density functions discussed above. For example, retracking Topex waveforms evidently shifts the main locus of data in Figure 6 toward Jason, resulting in more consistent means. Differences of the form (Jason minus Topex) have positive skewness, consistent with a wider spread of Jason data off the diagonal of Figure 5.

Pearson's coefficient of correlation  $\rho$  and the rms differences, both tabulated in Table 2, reflect the relative levels of agreement between the various data types seen previously. The rms difference between either altimeter and the numerical model is approximately 72 cm. This is slightly larger than the rms difference reported by Tolman et al. (2002) between the model and the wave heights measured by the ERS-2 satellite; adjusting the Jason data by the linear correction (2), combined with a similar adjustment for Topex (Lefèvre and Cotton, 2001), would presumably lower our rms

toward Tolman's reported value.

Regression coefficients are also given in Table 2 for the model wave heights relative to the satellite heights, again assuming equal error variances. For these cases this assumption of equal error is surely incorrect, but the resulting  $\beta_1$  yields a slope that is consistent with a principal component analysis and therefore usefully describes the slope of the major axis of an ellipse fitted to the observed data density (e.g., Bauer and Staabs, 1998). In that sense we see that the model agrees more closely with Topex than with Jason, even though the rms differences are nearly identical.

### **Buoy Comparisons**

Buoy comparisons have been routinely used to assess the  $H_s$  measurement capabilities of satellite altimeters (e.g., Monaldo, 1988). Most importantly, they have been used to establish calibration adjustments, generally in the form of linear corrections (e.g., Lefèvre and Cotton, 2001). We hesitate here to recommend such adjustments based on only 6 months of altimeter data and on a limited buoy dataset, but the buoy comparisons in this section clearly confirm some of the general features in the Jason altimeter data that have been noted above and are consistent for Topex data to earlier studies based on more extended datasets.

The buoy data employed here consist of hourly time series of significant wave heights measured at 20 moored buoys located in the deep ocean (see Figure 8). The buoys, operated and maintained by the U. S. National Data Buoy Center, use accelerometers or inclinometers to monitor wave motion, normally averaging data over 20 minutes for each reported hourly measurement. Quoted accuracies for  $H_s$  are  $\pm 0.2$  m. General statistics describing the wave environment at each buoy are summarized in Table 3. Note the typically enhanced energy with increasing latitude. The higher statistical moments of Table 1 (standard deviation, skewness, kurtosis) reassuringly fall within

the mid-ranges observed in Table 3. The first moment (the mean) of the buoy data, however, is somewhat less representative of the satellite-based averages. This is an unavoidable limitation of the buoy data, caused by their incomplete geographical coverage, especially the lack of data from the Southern Ocean. Useful conclusions can nonetheless still be obtained (and see also Bidlot et al., 2002).

An example  $H_s$  comparison time series, showing hourly buoy data from nearly 6 months and corresponding measurements from the two closest Jason tracks, is given in Figure 9. The satellite data are median filtered and further averaged over a distance of about 50 km near the buoy. The Jason data arrive in pairs every ten days, with occasional lacunae. The overall agreement between buoy and altimeter measurements appears impressive, although the time scale is admittedly too compressed for detailed comparisons.

Such details are more clearly revealed in the scatter diagrams of Figure 10 and in the summary statistics of Table 4. Figure 10 again shows a distorted distribution at small wave heights for Jason, which confirms suspicions noted above that the dearth of small waves must stem from some inadequacy in Jason waveform processing. In fact, Figure 10 suggests a slight curvature, or “hook,” in the scatter diagram, with lowest waves possibly mapped nonlinearly into higher reported waves.

Both Figure 10 and the mean differences in Table 4 suggest slightly better agreement with Topex than with Jason. Note the mean buoy/Topex difference is only 1 cm. Owing to the distribution of heights at the buoy locations, however, the Jason and Topex means are closer than for the global datasets of Tables 1 and 2.

For waves in the range 2–3 m, both Topex and Jason data are reporting wave heights slightly too small according to the buoy measurements. This behavior in Topex has been noted earlier by others (e.g., Gower, 1996; Lefèvre and Cotton, 2001). There are too few points in Figure 10 to

establish whether this discrepancy in  $H_s$  is a linear function over all wave heights (excluding for the moment the low Jason waves), but assuming that it is, Table 4 gives estimated slope and intercept parameters for the linear relationship. Because the estimates for Jason are likely influenced by the three obvious outliers in Figure 10 and by the odd behavior at small waves, we also show estimated parameters from an edited Jason-buoy dataset (with the outliers and all waves smaller than 1 meter removed). As before, the estimated parameters in Table 4 are based on orthogonal regression assuming equal error variances in both data type. If instead we assume no error in the buoy measurements, then the three estimates of  $\beta_1$  in Table 4 are:  $1.061 \pm 0.13$ ,  $1.130 \pm 0.18$ , and  $1.092 \pm 0.017$ , respectively. However, even perfect buoy measurements are point measurements and do not necessarily describe the wave environment over the surrounding region in the same way that an altimeter samples, and, of course, there is no reason to assume that the buoys are free from measurement error—Caires and Sterl (2003) recently concluded that buoys and altimeters have comparable error variances. For such reasons we prefer the  $\beta_1$  estimates of Table 4. The quoted standard errors are based on large-sample formulae given by Isobe et al. (1990) and have been checked by a bootstrap resampling calculation.

The  $\beta_i$  estimates of Table 4 can be used for linearly “adjusting” the altimetric wave-height data, in the manner done by Tolman et al. (2002) and by others. The 4.7% linear adjustment for Topex is consistent with that proposed by other investigators; both Gower (1996) and Lefèvre and Cotton (2001) recommend values close to 5%. The difference in  $\beta_1$  for Jason (edited) and Topex in Table 4 is 2.8%, which is quite consistent with the direct global comparisons above (2.7%, from Equation 1). We stress that our dataset is too limited to allow us to recommend use of such adjustment for large wave heights (greater than, say, 5 meters).

Finally, to complete the buoy comparisons we show in Figure 11 the joint density of  $H_s$  data

from the buoys and from the WaveWatch numerical model. The rms is 48 cm, which is smaller than the global rms between the model and the altimetry data, but this is probably due to the generally smaller wave environments at the buoy locations. Interestingly, there is again some distortion in the density contours at small wave heights, akin to that seen for Jason data. Some buoy systems are insensitive to extremely small waves and below a certain threshold will default to zero. But this appears not to have happened in our datasets except for one brief period (early July 2002) for buoy 42003 in the Gulf of Mexico where we inferred a threshold cutoff of 15 cm. Otherwise, the buoy data never report a completely calm ocean; the minimum  $H_s$  value for most buoys usually exceeds 50 cm (see minima tabulated in Table 3).

## Conclusions

We have here “validated” the significant wave heights from the Jason-1 altimeter, in the sense that the rms wave heights between Jason and Topex data and between Jason and buoy measurements are well below the mission specification of 0.5 meters. The near-simultaneous measurements with Topex have an rms of 21 cm, and application of median filters to remove outliers and reduce high-frequency noise reduces this rms to 15 cm. A linear adjustment of form (2) further reduces the rms to only 11 cm, which is nearly the precision of the original Topex data.

The extensive collinear Jason-Topex dataset shows a mean  $H_s$  discrepancy of 9 cm. Although buoy comparisons suggest that Topex data may be the more accurate, the mean discrepancy is nonetheless halved when Topex waveforms are retracked. The collinear data show a systematic trend between Jason and Topex, with most Jason wave heights lower than Topex by 2.7%. The Jason measurements are also somewhat more prone to noise and outliers, which are manifested by the warped contours in the joint density function (Figures 5 and 6).

Buoy comparisons do confirm that a linear adjustment to the Jason data slightly larger than that commonly used for Topex is warranted, but more extensive comparison datasets that contain larger wave heights are needed. The most problematic aspect of the Jason-1 dataset is the dearth of measured small waves. In general, however, the Jason data are of high quality and are capable of extending the valuable 11-year global time series generated by (and, as of this writing, continuing to be generated by) the Topex/Poseidon mission.

*Acknowledgments.* We thank Phil Callahan for providing his dataset of retracked Topex data and for useful discussions. This work was funded by the U. S. National Aeronautics and Space Administration under a Jason-1 science investigation.

## References

- Athanassoulis, G. A., and C. N. Stefanakos (1995). A nonstationary stochastic model for long-term time series of significant wave height. *Journal of Geophysical Research*, 100: 14149–14162.
- Bacon, S., and D. J. T. Carter (1991). Wave climate changes in the North Atlantic and North Sea. *International Journal of Climatology*, 11: 545–558.
- Bauer, E., K. Hasselmann, I. R. Young, and S. Hasselmann (1996). Assimilation of wave data into the wave model WAM using an impulse response function method. *Journal of Geophysical Research*, 101: 3801–3816.
- Bauer, E. and C. Staabs (1998). Statistical properties of global significant wave heights and their use for validation. *Journal of Geophysical Research*, 103: 1153–1166.
- Bidlot, J.-R., D. J. Holmes, P. A. Wittmann, R. Lalbeharry, and H. S. Chen (2002). Intercomparison of the performance of operational ocean wave forecasting systems with buoy data. *Weather and Forecasting*, 17:287–310.
- Caires, A. and A. Sterl (2003). Validation of ocean wind and wave data using triple collocation. *Journal of Geophysical Research*, 108(C3): 3098.
- Callahan, P. S., C. S. Morris, and S. V. Hsiao (1994). Comparison of Topex/Poseidon  $\sigma_0$  and significant wave height distributions to Geosat. *Journal of Geophysical Research*, 99: 25015–25024.
- Cheng, C.-L., and J. W. Van Ness (1999). *Statistical Regression with Measurement Error*. Arnold, London.
- Dumont, J. P., P. Sicard, J. Stum, and O. Z. Zanife (2001). Centre Multi-missions Altimétrique (CMA) Altimeter Level 2 Processing, CNES, Toulouse, 427 pp.
- Fedor, L. S., T. W. Godbey, J. F. R. Gower, R. Guptill, G. S. Hayne, C. L. Rufenach, and E. J. Walsh (1979). Satellite measurements of sea state: an algorithm comparison. *Journal of Geophysical Research*, 87: 3991–4001.
- Gower, J. F. R. (1996). Intercalibration of wave and wind data from Topex/Poseidon and moored buoys off

- the west coast of Canada. *Journal of Geophysical Research*, 101: 3817–3829.
- Hosking, J. R. M. (1985). Maximum-likelihood estimation of the parameters of the generalized extreme-value distribution. *Applied Statistics*, 34: 301–310.
- Hosking, J. R. M. and J. R. Wallis (1997). *Regional Frequency Analysis: An Approach Based on L-Moments*. Cambridge Univ. Press, Cambridge.
- Isobe, T., E. D. Feigelson, M. G. Akritas, and G. J. Babu (1990). Linear regression in astronomy. *Astrophysical Journal*, 364: 104–113.
- Johnson, N. L., S. Kotz, and N. Balakrishnan (1995). *Continuous Univariate Distributions*, Vol. 2. Wiley, New York.
- Lefèvre, J.-M., and P. D. Cotton (2001). Ocean surface waves. In *Satellite Altimetry and Earth Sciences*, (Eds.: L.-L. Fu and A. Cazenave), Chapter 7, pp. 305–328. Academic Press, San Diego.
- Lionello, P. and P. A. E. M. Janssen (1992). Assimilation of altimeter wave data in a global third generation wave model. *Journal of Geophysical Research*, 97: 14453–14474.
- Madansky, A. (1959). The fitting of straight lines when both variables are subject to error. *Journal of the American Statistical Association*, 54: 173–205.
- Monaldo, F. (1988). Expected differences between buoy and radar altimeter estimates of wind speed and significant wave height and their implications on buoy-altimeter comparisons. *Journal of Geophysical Research*, 93: 2285–2302.
- Moran, P. A. P. (1971). Estimating structural and functional relationships. *Journal of Multivariate Analysis*, 1: 232–255.
- Ochi, M. K. (1998). *Ocean Waves: The Stochastic Approach*. Cambridge Univ. Press, Cambridge.
- Quarty, G. (1997). Achieving accurate altimetry across storms: improved wind and wave estimates from C band. *Journal of Atmospheric and Oceanic Technology*, 14: 705–715.
- Rodríguez, E. and J. M. Martin (1994). Assessment of the Topex altimeter performance using waveform

- retracking. *Journal of Geophysical Research*, 99: 24957–24969.
- Tolman, H. L. (1999). User manual and system documentation of WaveWatch III version 1.18. NOAA/NCEP Tech. Note 166, 110 pp.
- Tolman, H. L., B. Balasubramaniyan, L. D. Burroughs, D. V. Chalikov, Y. Y. Chao, H. S. Chen, and V. M. Gerald (2002). Development and implementation of wind-generated ocean surface wave models at NCEP. *Weather and Forecasting*, 17: 311–333.
- Tournadre, J. (1993). Time and space scales of significant wave heights. *Journal of Geophysical Research*, 98: 4727–4738.
- Wang, X. L. and V. R. Swail (2001). Changes in extreme wave heights in northern hemisphere oceans and related atmospheric circulation regimes. *Journal of Climate*, 14: 2204–2221.

Table 1: Global  $H_s$  statistics

	Mean (cm)	Median (cm)	Mode (cm)	Std. dev. (cm)	Skewness	Kurtosis
Topex	272	240	191	132	1.39	2.64
Topex (retracked)	268	236	189	133	1.36	2.46
Jason-1	263	232	187	128	1.36	2.51
WaveWatch-III	281	252	202	131	1.22	2.10

From 6 million 1-Hz measurements (or predictions) along satellite ground-track.

Table 2: Global statistics of  $H_s$  differences

	Mean	RMS	Skewness	Linear relationship		$\rho$
	(cm)	(cm)		$\beta_0$	$\beta_1$	
Jason / Topex	-8.9	21	1.73	-2	0.974	0.990
Retracked / Topex	-4.1	10	-0.10	-7	1.009	0.997
Jason / Model	-18.0	73	0.61	-12	0.979	0.850
Topex / Model	-9.1	72	0.82	-11	1.006	0.854

For comparison A/B, the mean and skewness refer to  $(A - B)$ , while the linear structural relationship describes  $A = \beta_1 B + \beta_0$  (in cm) assuming equal error variances in A and B.

Statistics based on 6 million 1-Hz measurements (or predictions) along satellite ground-track.

Table 3: Buoy  $H_s$  statistics

WMO ID	Location		Mean (cm)	Mode (cm)	Median (cm)	Stdev (cm)	Skew	Kurt	Min (cm)	Max (cm)
51028	0.00°N	153.86°W	191	190	191	37	0.08	-0.40	99	302
51002	17.19°N	157.83°W	247	230	242	56	0.73	0.99	116	489
51004	17.44°N	152.52°W	247	230	238	57	1.09	2.04	111	539
51003	19.17°N	160.73°W	219	210	208	61	1.38	2.99	98	604
51001	23.40°N	162.27°W	243	200	220	89	1.56	3.43	86	780
42002	25.89°N	93.57°W	135	100	119	79	1.53	3.21	23	584
42001	25.92°N	89.68°W	113	80	93	77	2.41	12.20	17	1120
42003	25.94°N	85.91°W	108	60	90	74	2.02	5.75	15	657
41010	28.89°N	78.52°W	155	100	139	69	1.31	2.48	40	537
41002	32.28°N	75.20°W	176	140	155	86	1.79	4.29	52	690
41001	34.68°N	72.64°W	197	130	167	106	1.64	3.32	50	833
46059	37.98°N	130.00°W	259	170	231	133	2.21	7.03	86	1076
44004	38.46°N	70.69°W	201	100	170	119	1.61	3.71	46	1064
46006	40.84°N	137.49°W	278	160	230	167	1.80	4.37	69	1423
44011	41.09°N	66.59°W	192	100	158	120	1.67	3.11	47	857
46002	42.53°N	130.26°W	277	160	239	144	1.55	3.14	69	1234
46005	46.06°N	131.02°W	279	160	238	156	1.41	2.19	68	1152
46066	52.67°N	155.00°W	289	230	255	151	1.26	2.23	67	1099
46001	56.30°N	148.17°W	270	150	236	145	1.11	1.25	58	999
46035	56.91°N	177.81°W	276	230	243	155	1.01	0.74	37	896

Table 4: Altimeter-buoy  $H_s$  differences

	Mean	RMS	Skewness	Linear relationship		$\rho$
	(cm)	(cm)		$\beta_0$	$\beta_1$	
Topex	-1.0	16.8	0.0	$-7.0 \pm 2.0$	$1.046 \pm 0.013$	0.985
Jason	-4.5	30.0	68.5	$-10.0 \pm 4.3$	$1.082 \pm 0.030$	0.954
Jason (edited)	-11.1	21.1	-0.4	$-3.5 \pm 3.0$	$1.074 \pm 0.017$	0.982

The mean and skewness refer to (altimeter minus buoy). The linear structural relationship corresponds to  $\text{Buoy} = \beta_1 \times \text{Altimeter} + \beta_0$  (in cm), assuming equal error variances. Corresponds to data shown in Figure 10.

## Figure Captions

Figure 1. (Top) Observed  $H_s$  measurements by Jason-1 (ragged line) along a satellite path across the Pacific Ocean and into the South Atlantic (see map inset). The corresponding WaveWatch numerical model output is shown by the heavy, smooth line. Horizontal axis is time since previous ascending node; actual time at the beginning of shown data segment is 2002 Feb 7, 07:02 UT. Distance can be reckoned from satellite ground speed of approximately  $5.75 \text{ km s}^{-1}$ . (Bottom) A zoom view of part of the arc, also showing corresponding data from the Topex altimeter, offset by 1 meter for clarity.

Figure 2. Coherence  $\gamma^2$  between Topex and Jason  $H_s$  data shown in Figure 1. Computed by Welsh's method of segment averaging (33 segments). Linear interpolation has been used across any small gaps in the two time series.

Figure 3. Observed density functions of significant wave heights for the period February–July 2002. The WaveWatch model (Tolman, 2002) has been sampled in the same way as the measured data along the satellite track. Insets show zoom views for larger wave heights. The dotted line is the probability density of a generalized extreme value distribution (Hosking, 1985) fitted to the retracked Topex distribution; to facilitate comparisons, it is replotted in identical fashion in each panel.

Figure 4. Cumulative distribution of the Topex- and Jason-observed significant wave heights for February–July 2002. The vertical axis is such that a lognormal distribution would appear as a straight line; the dotted line is straight and is shown for comparison purposes. The shading

denotes region containing  $\pm 1 \sigma$ , or 68% of the data.

Figure 5. Observed joint density function of Jason and Topex  $H_s$  measurements, from six months of observations during the Jason verification campaign. Contours are roughly logarithmic: 0.0003, 0.001, 0.003, 0.01, 0.03, 0.1, 0.3, 1.0  $\text{m}^{-2}$ .

Figure 6. As in Figure 5 except the difference (Topex minus Jason) is plotted as a function of Jason-observed  $H_s$  and data are median filtered. The dotted line is the estimated linear structural relationship assuming equal measurement errors in Topex and Jason. (a) Original Topex data; (b) Retracked Topex data.

Figure 7. As in Figure 5 but for model predictions from WaveWatch III (Tolman et al., 2002) versus Jason measurements. For six months of observations/predictions. Wave model is evaluated by trilinear interpolation to the satellite space-time point.

Figure 8. Buoys used for wave-height comparisons.

Figure 9. Time series of hourly  $H_s$  measurements at buoy 46001 in Gulf of Alaska. Open circles are Jason-1  $H_s$  measurements at times of flyby along two nearby tracks (see map inset).

Figure 10. Scatter diagrams comparing Jason and Topex  $H_s$  measurements with near-simultaneous buoy measurements. There are 336 comparison points for Jason, 399 for Topex.

Figure 11. Observed joint probability density of model-predicted  $H_s$  versus buoy measurements,

based on hourly data from the 20 buoys shown in Figure 8 over the period January–August 2002. Contours are 0.003, 0.01, 0.03, 0.1, 0.3, and 0.6 m<sup>-2</sup>. The rms difference over all pairs is 48 cm; the correlation coefficient is 0.913. More extensive comparisons can be found in Tolman et al. (2002).

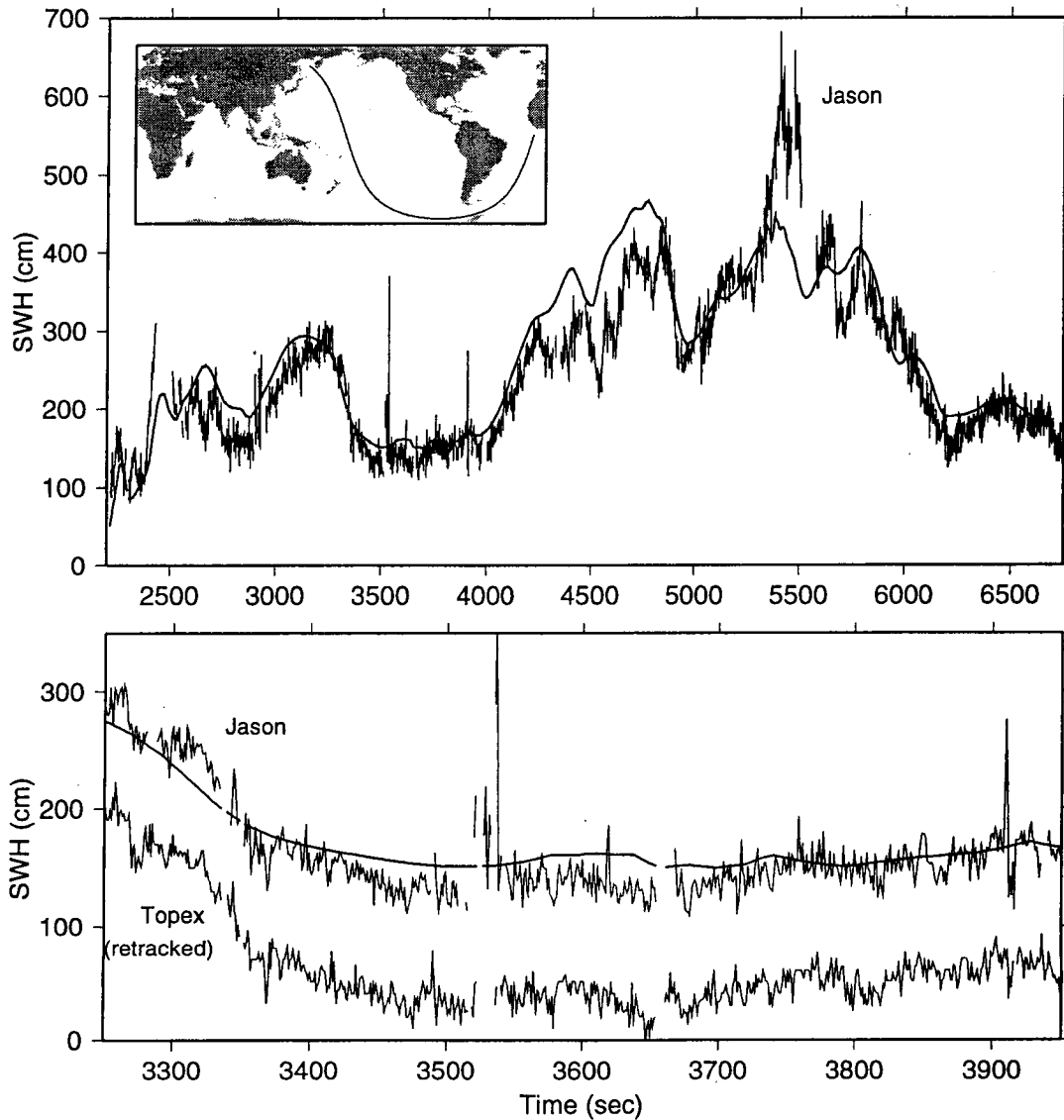


Figure 1: (Top) Observed  $H_s$  measurements by Jason-1 (ragged line) along a satellite path across the Pacific Ocean and into the South Atlantic (see map inset). The corresponding WaveWatch numerical model output is shown by the heavy, smooth line. Horizontal axis is time since previous ascending node; actual time at the beginning of shown data segment is 2002 Feb 7, 07:02 UT. Distance can be reckoned from satellite ground speed of approximately  $5.75 \text{ km s}^{-1}$ . (Bottom) A zoom view of part of the arc, also showing corresponding data from the Topex altimeter, offset by 1 meter for clarity.

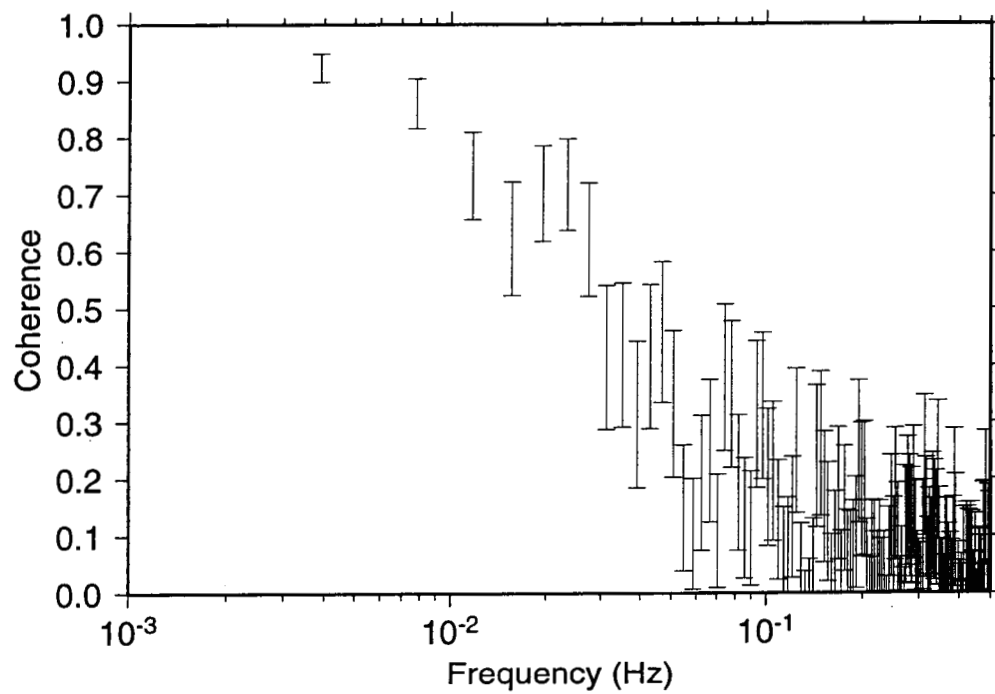


Figure 2: Coherence  $\gamma^2$  between Topex and Jason  $H_s$  data shown in Figure 1. Computed by Welsh's method of segment averaging (33 segments). Linear interpolation has been used across any small gaps in the two time series.

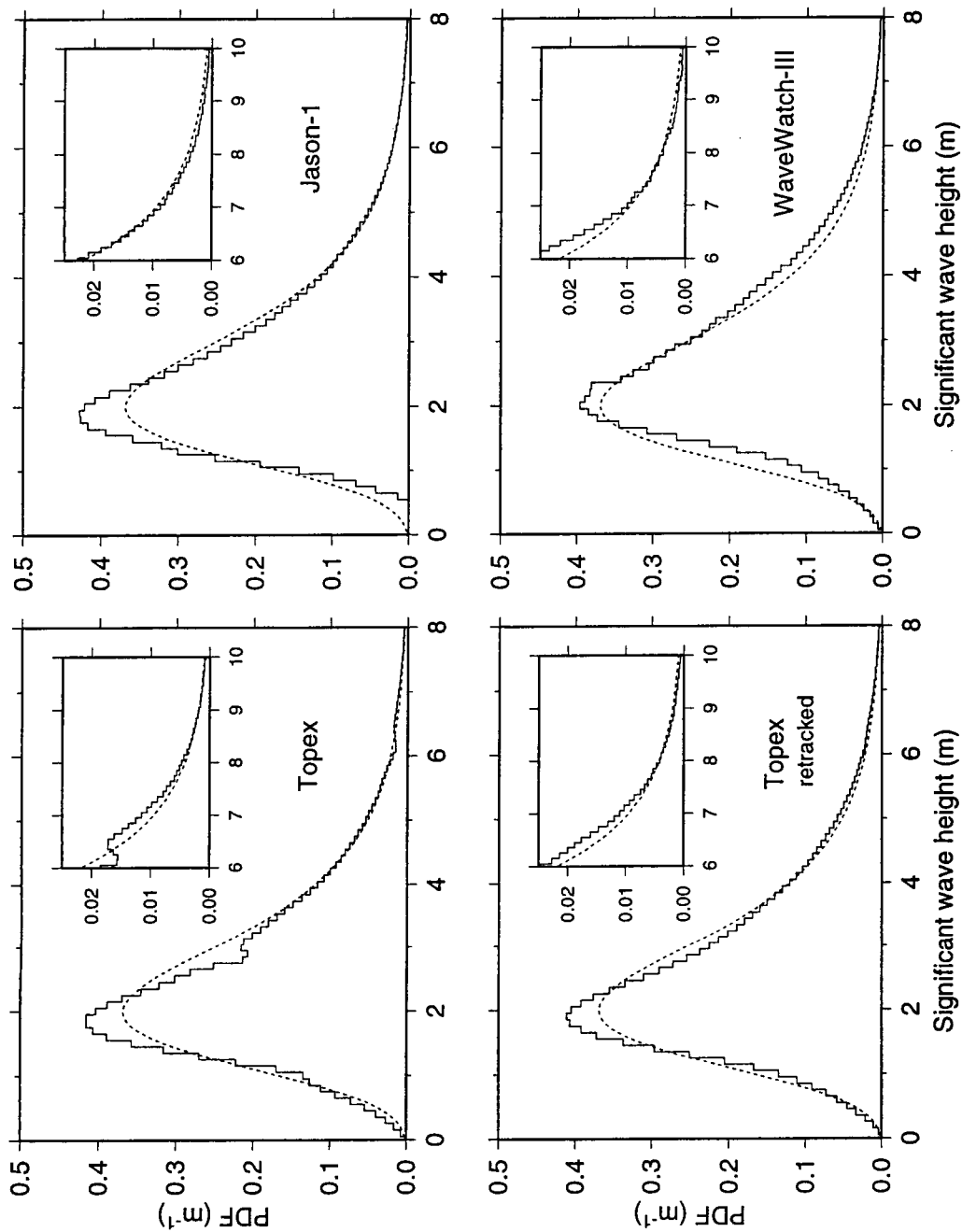


Figure 3: Observed density functions of significant wave heights for the period February–July 2002. The WaveWatch model (Tolman, 2002) has been sampled in the same way as the measured data along the satellite track. Insets show zoom views for larger wave heights. The dotted line is the probability density of a generalized extreme value distribution (Hosking, 1985) fitted to the retracked Topex distribution; to facilitate comparisons, it is replotted in identical fashion in each panel.

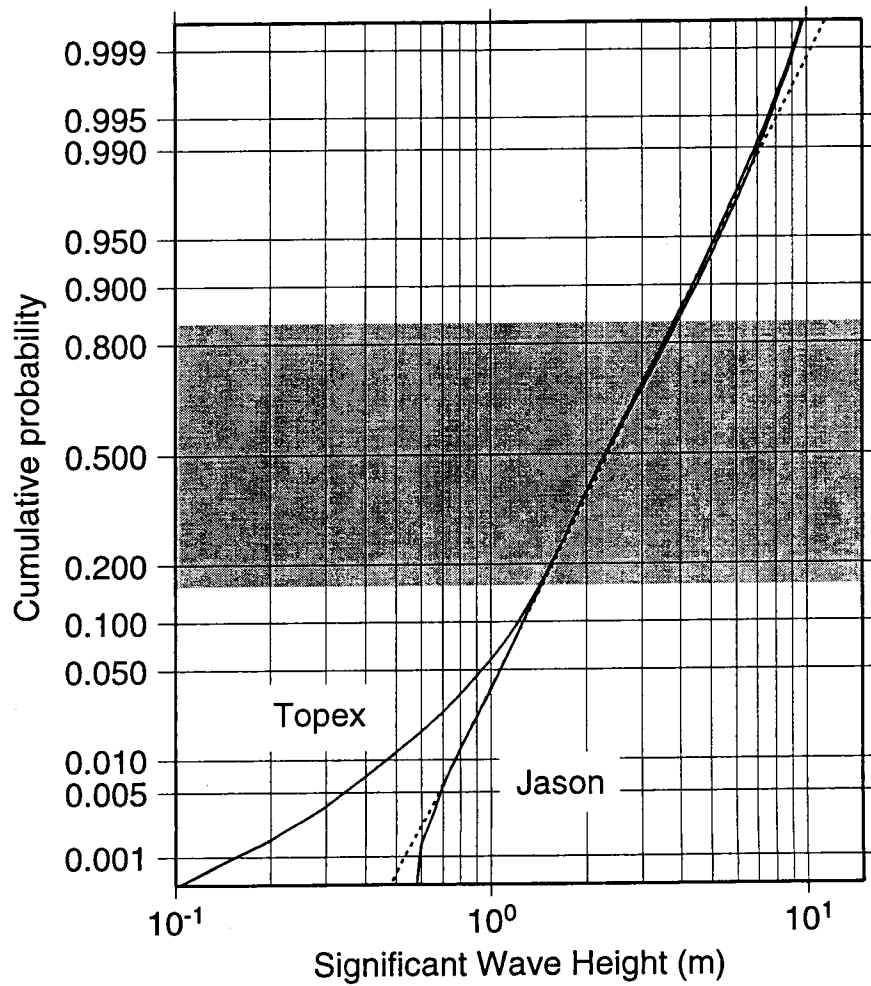


Figure 4: Cumulative distribution of the Topex- and Jason-observed significant wave heights for February–July 2002. The vertical axis is such that a lognormal distribution would appear as a straight line; the dotted line is straight and is shown for comparison purposes. The shading denotes region containing  $\pm 1\sigma$ , or 68% of the data.

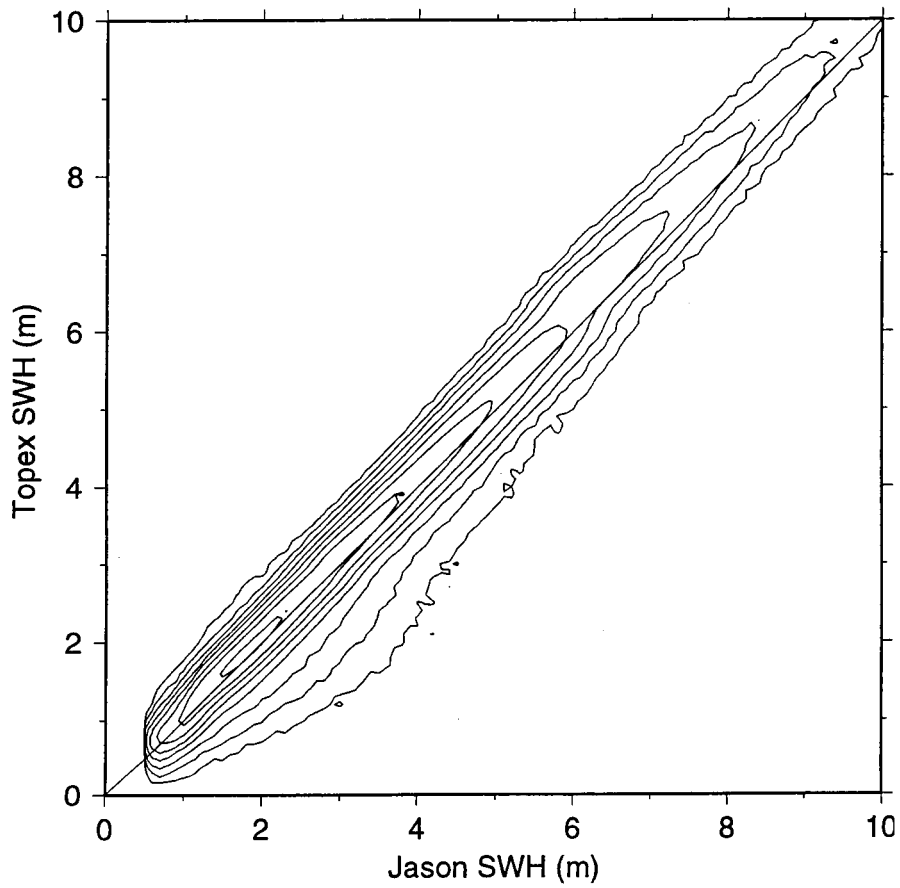


Figure 5: Observed joint density function of Jason and Topex  $H_s$  measurements, from six months of observations during the Jason verification campaign. Contours are roughly logarithmic: 0.0003, 0.001, 0.003, 0.01, 0.03, 0.1, 0.3, 1.0  $\text{m}^{-2}$ .

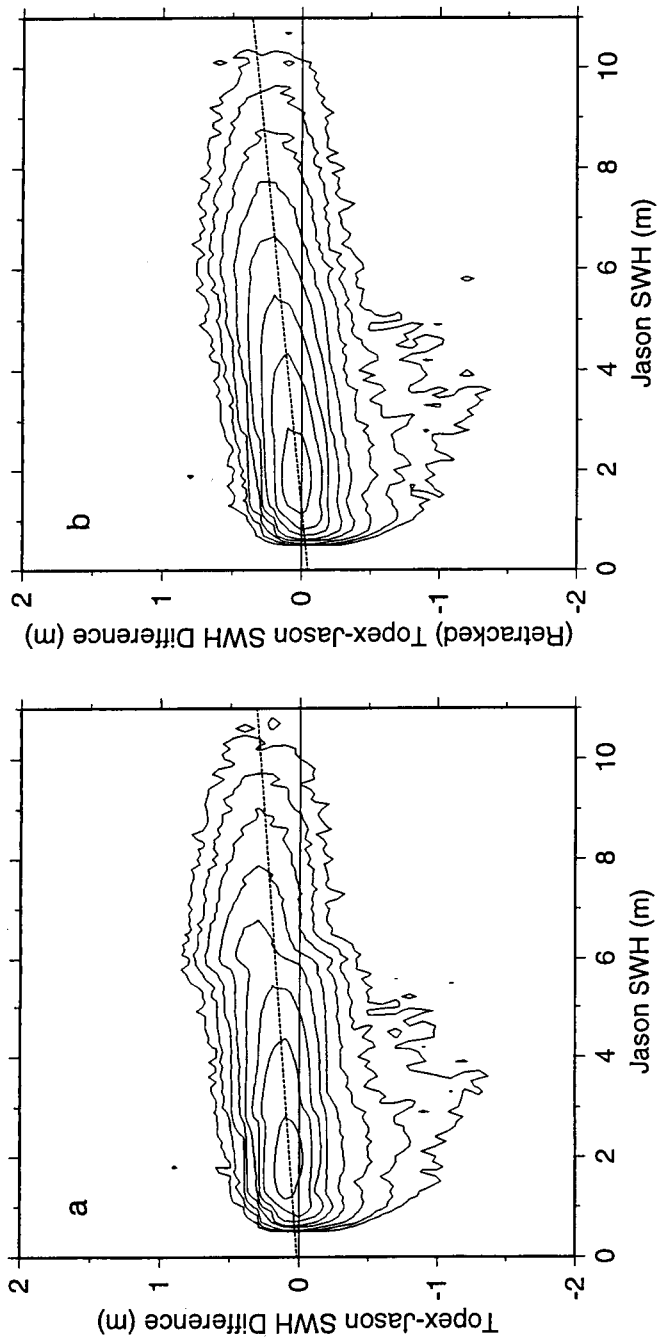


Figure 6: As in Figure 5b except the difference (Topex minus Jason) is plotted as a function of Jason-observed  $H_s$  and data are median filtered. The dotted line is the estimated linear structural relationship assuming equal measurement errors in Topex and Jason. (a) Original Topex data; (b) Retracked Topex data.

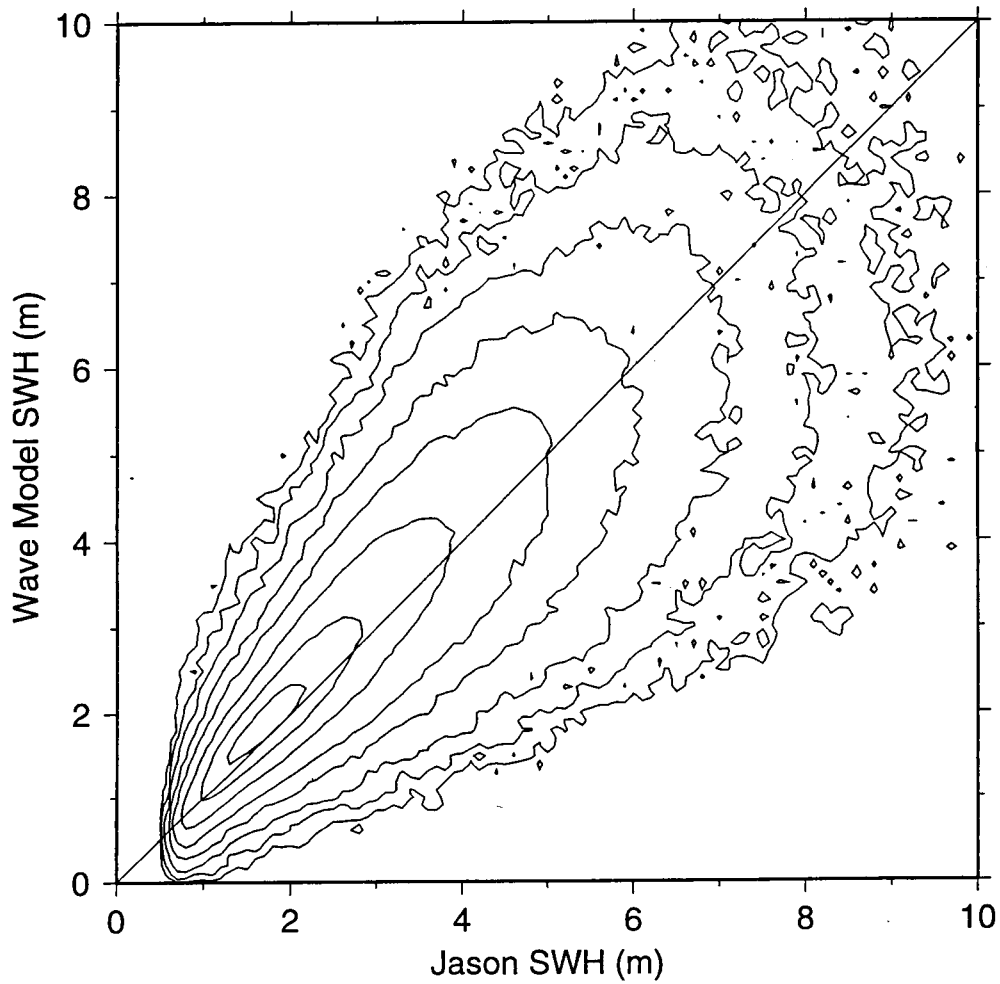


Figure 7: As in Figure 5 but for model predictions from WaveWatch III (Tolman et al., 2002) versus Jason measurements. For six months of observations/predictions. Wave model is evaluated by trilinear interpolation to the satellite space-time point.

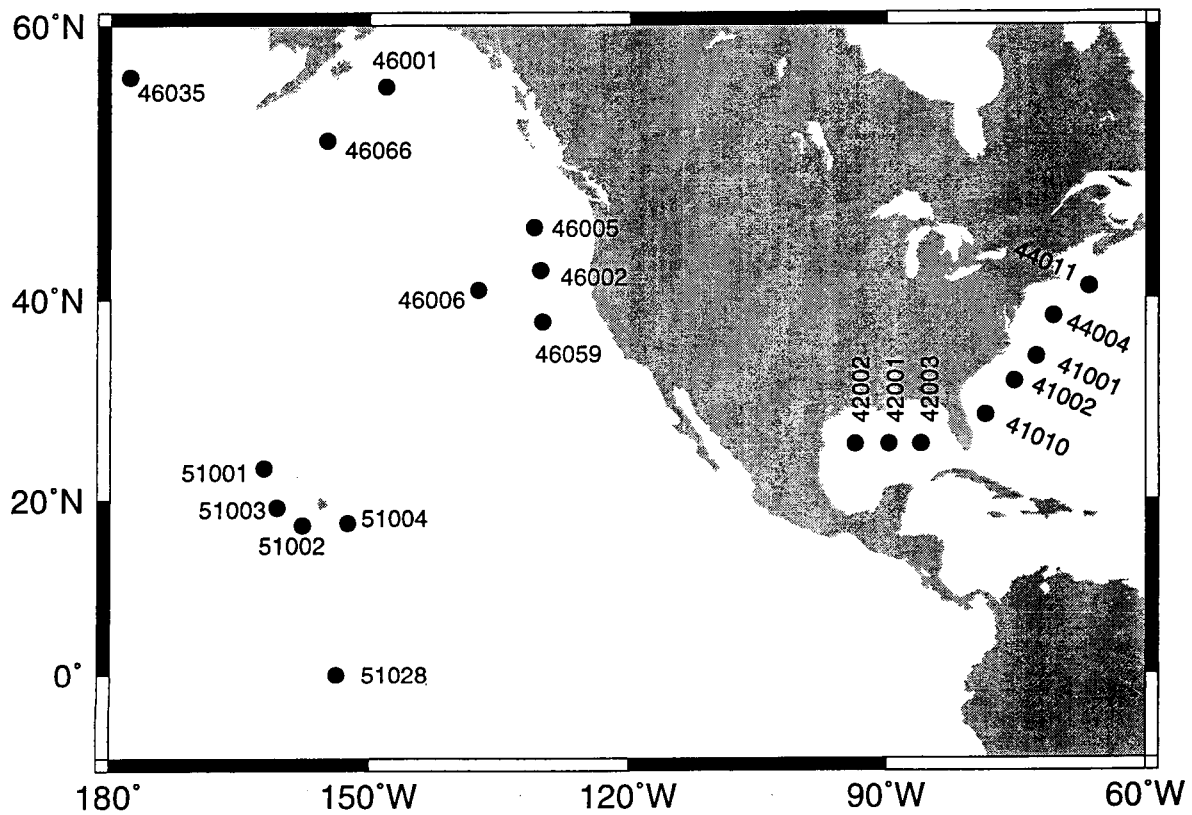


Figure 8: Buoys used for wave-height comparisons.

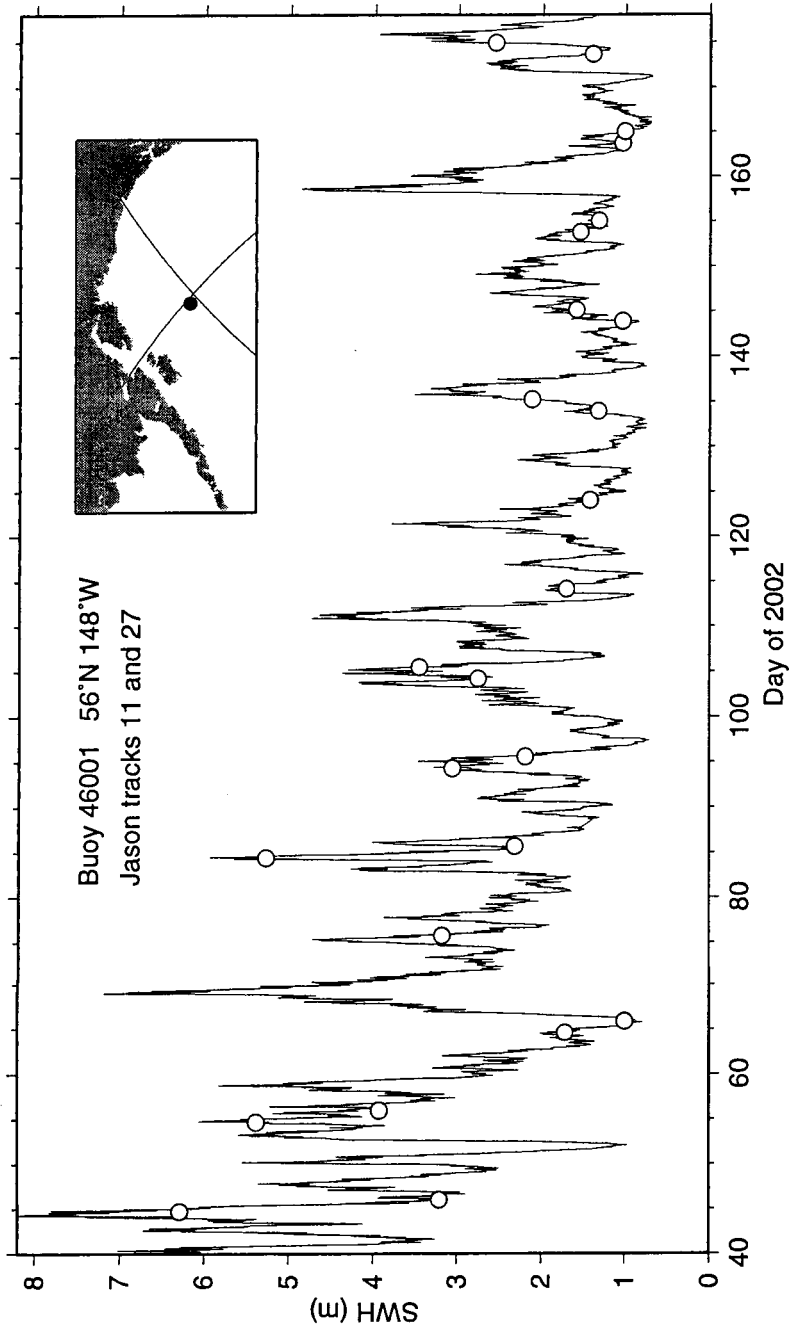


Figure 9: Time series of hourly  $H_s$  measurements at buoy 46001 in Gulf of Alaska. Open circles are Jason-1  $H_s$  measurements at times of flyby along two nearby tracks (see map inset).

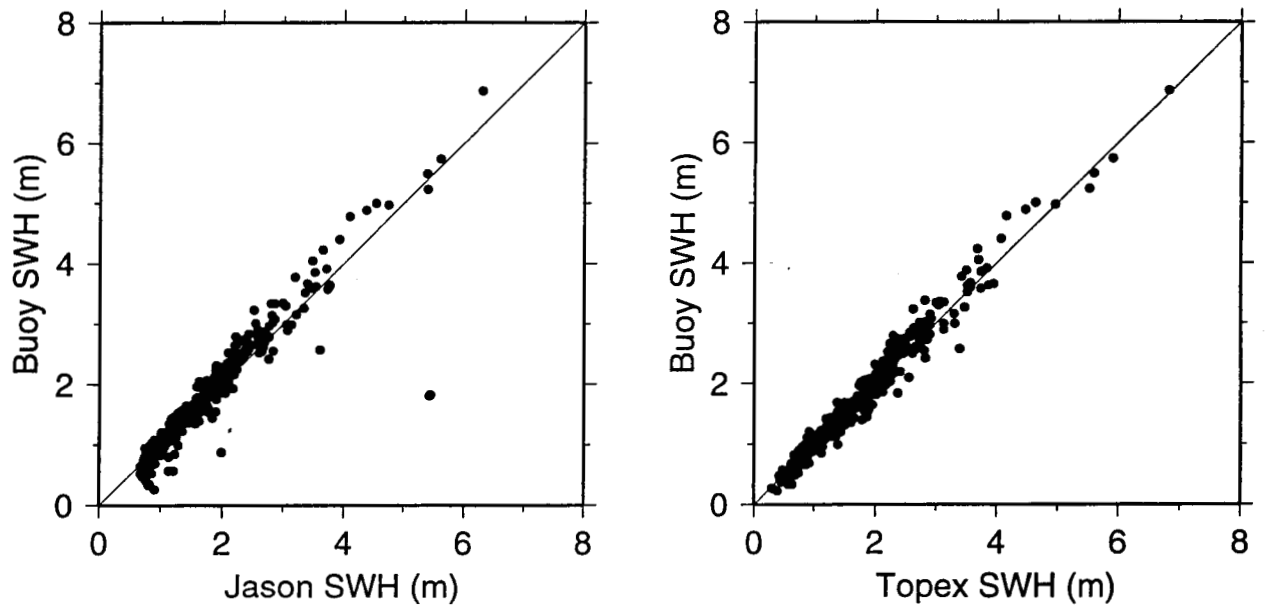


Figure 10: Scatter diagrams comparing Jason and Topex  $H_s$  measurements with near-simultaneous buoy measurements. There are 336 comparison points for Jason, 399 for Topex.

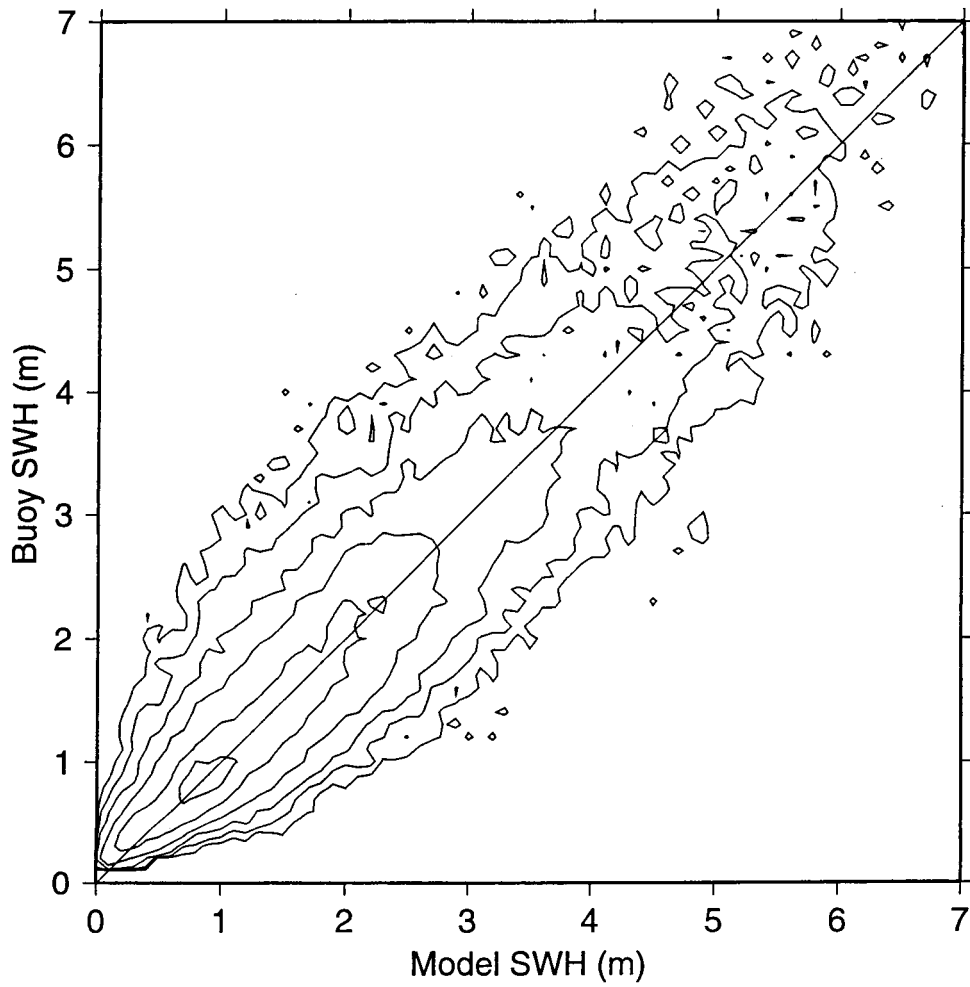


Figure 11: Observed joint probability density of model-predicted  $H_s$  versus buoy measurements, based on hourly data from the 20 buoys shown in Figure 8 over the period January–August 2002. Contours are 0.003, 0.01, 0.03, 0.1, 0.3, and 0.6  $\text{m}^{-2}$ . The rms difference over all pairs is 48 cm; the correlation coefficient is 0.913. More extensive comparisons can be found in Tolman et al. (2002).